Available online at www.sciencedirect.com

ScienceDirect

Advances in Space Research 66 (2020) 1647–1658

ADVANCES IN SPACE RESEARCH (a COSPAR publication)

www.elsevier.com/locate/asr

Improved weighting scheme using consumer-level GNSS L5/E5a/B2a pseudorange measurements in the urban area

Hoi-Fung Ng [a], Guohao Zhang [a,*], Kai-Yuan Yang [b], Shi-Xian Yang [b], Li-Ta Hsu [a]

[a] *Interdisciplinary Division of Aeronautical and Aviation Engineering, Hong Kong Polytechnic University, Kowloon, Hong Kong*
[b] *Allystar Technology Co. Ltd., New Territories, Hong Kong*

Received 3 March 2020; received in revised form 1 June 2020; accepted 2 June 2020
Available online 11 June 2020

Abstract

The accurate global navigation satellite system (GNSS) positioning in the dense urban areas is still a challenge, especially for low-cost receivers. The multipath effects and non-line-of-sight (NLOS) receptions from surrounding buildings will significantly degrade the positioning performance. Due to the increasing channel number in GNSS chip, the low-cost receiver tends to be capable of acquiring multi-frequency signals, including the new L5-band signal. Because of the higher chipping rate, the GNSS L5-band measurement is less affected by the multipath effect, whereas the measurement number is limited in the current stage. On the contrary, the availability of the conventional L1-band measurement is sufficient to achieve a good dilution of precision (DOP). Based on the complementary characteristics, a GNSS L1/L5 bands integrated positioning algorithm is developed in this study to improve the positioning performance in urban areas. A modified weighting model based on carrier-to-noise ratio and satellite elevation angle is employed to assign proper weighting between L1-band and L5-band measurements. Meanwhile, the dMP5 feature from dual-frequency measurement and the consistency check algorithm are employed to detect and exclude outliers, which are possibly NLOS receptions. Experimental results and analyses indicate that the developed DFE-CCWLS method can significantly improve the positioning accuracy, achieving the root-mean-square error less than 10 m for most of the urban scenarios.

Keywords: GNSS; Multipath; Urban Canyon; GNSS L5-band

1. Introduction

Most public or private services nowadays utilize the location information from users to improve efficiency and quality, namely the location-based service (LBS) (Küpper, 2005). Among various positioning systems, the global satellite navigation system (GNSS) provides a global coverage satellite-based positioning, navigation, and timing service. As the only approach providing all-weather absolute positioning solutions, the GNSS plays an essential role in LBS (Chen et al., 2017). The performance of LBS tightly relies on the accuracy of the positioning system (Türk, 2006). In open-sky areas, the GNSS is capable of achieving a sub-meter-level positioning accuracy (Basiri et al., 2014), which satisfies most of the LBSs. However, GNSS positioning accuracy can be easily affected by the environment.

In urban areas, the multipath (MP) effect and the non-line-of-sight (NLOS) reception are the main issues degrading the GNSS performance (Zhu et al., 2018). For the MP effect, the receiver receives not only the direct satellite signal, but also the reflected signals from nearby building surfaces. A statistical analysis shows the MP delay follows a Gamma distribution (Chen, 2018). The NLOS reception only receives the reflected signal while the direct signal is

* Corresponding author.
E-mail addresses: ivannhf.ng@connect.polyu.hk (H.-F. Ng), guo-hao.zhang@connect.polyu.hk (G. Zhang), lt.hsu@polyu.edu.hk (L.-T. Hsu).

https://doi.org/10.1016/j.asr.2020.06.002
0273-1177/

blocked by the obstacles (Groves, 2013). The additional traveling distance of the reflected signals will introduce enormous errors in the GNSS pseudorange measurements. Without proper error mitigation techniques, the positioning accuracy can be degraded with over 50 m error (Hsu, 2018).

An applicable MP effect mitigation approach is to employ GNSS L5-band measurements. The L5-band signal is designed with a higher chipping rate (shorter chip length) comparing to that of the L1-band signal (Leclère et al., 2018). As the characteristic of autocorrelation of Gold code, the reflected signal with a delay exceeding a chip length has no interference to the GNSS pseudorange measurement. In the other words, reflected signal coming from about 30 and 300 m away have no impact on L5-band and L1-band, respectively. In theory, the L5-band signal naturally has a much better resistibility to multipath comparing to that of the conventional L1-band signal (Spilker and Van Dierendonck, 2001).

Besides, the GNSS L5-band measurements are already available on the low-cost consumer-level receivers. The GNSS signal band currently used in the low-cost receiver is shown in Fig. 1. Usually, the commercial receiver capable of receiving the L1 C/A, B1I and E1 signals from GPS/QZSS, BDS, and Galileo, respectively. For the latest receiver employing the lower L-band signal (1176.45 MHz), it is capable of receiving L5, B2a and E5a signals in addition to the preceding signals. The combination of GPS/ Galileo /BDS can also achieve a satisfactory satellite geometrical distribution for positioning (Zhang et al., 2019). Therefore, the GNSS L5-band signal has excellent potential to contribute to civilian positioning applications. The remaining issue is how to make use of the benefits from the L5-band signals.

In this paper, a new GNSS L1/L5 bands integrated positioning algorithm is developed to improve the positioning performance in the urban areas. The contributions of the developed system are threefold: (1) the GNSS L1-band and L5-band signals are complementarily integrated by a modified weighted-least-square approach to mitigate the MP effect; (2) the dMP5 feature is extracted from the dual-frequency measurements to detect and exclude outliers before positioning; (3) L1/L5 bands integrated consistency check is employed to detect and isolate outliers during positioning.

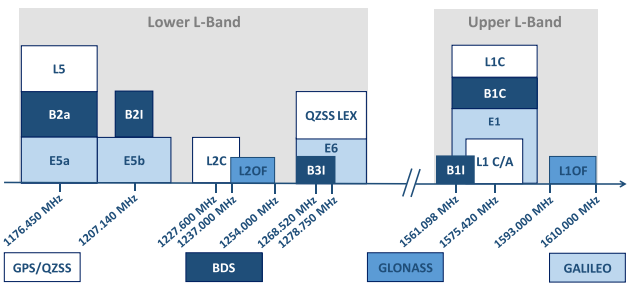

Fig. 1. Spectrum of GNSS signals band.

The remainder of this paper is organized as follows: Section 2 gives the related literature review. Section 3 details the features that we used to detect MP effects. The L1/L5 bands integrated positioning algorithm is given in Section 4, which is followed by experiment setup and results. Finally, the concluding remarks and future work are summarized.

2. Research background

For the MP or NLOS effect mitigation, a traditional method is to adjust the weighting of each GNSS measurement during positioning based on the carrier-to-noise ratio (C/N_0) and elevation angle (Realini & Reguzzoni, 2013). By testing the measurement residual during positioning, the outliers can be detected and excluded from measurements (Groves & Jiang, 2013; Hsu et al., 2015b). Since the NLOS and MP effects are caused by the signals reflecting from the building surface, many recent studies utilize the 3D building model to mitigate those effects, namely the 3D mapping aided (3DMA) GNSS. The 3DMA GNSS shadow matching conducts positioning by matching the satellite visibility with the building boundary (Wang et al., 2015). Moreover, the 3DMA GNSS ray-tracing corrects the NLOS delay by simulating the reflected signal with the 3D building model, achieving the positioning performance with less than 10 m error (Hsu et al., 2016). However, besides requiring a large scale of the 3D building model, the 3DMA GNSS also significantly increases the computational load (Ng et al., 2019).

From the hardware perspective, the antenna array can adjust its gain pattern to isolate the reflected signals, namely the beamforming technique (Nobuaki et al., 2017; Seco-Granados et al., 2005). The antenna with a wave-absorbing shield can also mitigate the MP effect (Ge et al., 2019). Furthermore, the direct GNSS signal is right-handed circular polarization (RHCP), while the reflected signal will be shifted to left-handed circular polarization (LHCP). Therefore, a dual-polarization antenna can distinguish the reflected signal from the direct signal and mitigates its effect (Groves et al., 2010; Jiang & Groves, 2014). However, these methods only partially mitigate the NLOS and MP effects, while requiring additional devices.

Instead of aided by additional information or devices, the GNSS L5-band measurement is designed with a better positioning behavior naturally. In addition to a higher chipping rate as 10.23 Mchip/s (Leclère et al., 2018), the L5-band signal also has a shorter wavelength to reduce the waveform distortion. As a result, the L5-band signal can achieve a higher accuracy on the code and carrier phase measurements (Lohan & Borre, 2016; Meurer et al., 2009). The advantages of employing the L5 signal-to-noise ratio for multipath reflectometry are also investigated (Tabibi et al., 2015). Moreover, the L5-band signal experiences a different ionospheric delay than the L1-band signal, due to the different wavelengths (Leick et al., 2015). The ionospheric delay can be eliminated by the linear combination

of dual-frequency signals (van der Marel & de Bakker, 2012). The L1/L2/L5 bands triple frequency measurement has great potential to improve the performance of single-point-positioning (Li et al., 2013) or the advanced receiver autonomous integrity monitoring (El-Mowafy, 2017). Besides, the GNSS precise point positioning technique (PPP) has been developed to achieve centimeter-level positioning accuracy (Zumberge et al., 1997). The triple frequency measurement can be applied to PPP, achieving faster convergence (Deo & El-Mowafy, 2018; Guo et al., 2016). The benefits of the L5 signal have also been employed by the high-end multi-frequency geodetic receiver (Spilker and Van Dierendonck, 2001), in order to perform better PPP (Qin et al., 2019) or real-time kinematic (RTK) positioning (Luo et al., 2016). Moreover, GNSS signals with different wavelengths will behave differently on the C/N_0 of the multipath affected signals. This characteristic has been utilized as a feature to detect the MP effect for the geodetic GNSS receiver in the urban area (Strode & Groves, 2016).

Recently, the acquisition of GNSS L5-band signal is available on the new generation low-cost receiver, aiming to provide a better positioning performance. Even for the smartphone, the positioning accuracy can be improved by double differencing the dual-frequency measurements with a reference receiver (Warnant et al., 2018). Another study also shows that the multi-constellation dual-frequency measurements provide more accurate clocks and orbital data for smartphones (Crosta et al., 2018). However, the total number of the L5-band signals available is limited in the current stage, especially for the urban scenario with building blockage. It may distort the dilution of precision (DOP) and degrades the positioning performance (Hsu et al., 2015a). Therefore, it is necessary to develop a positioning strategy utilizing the benefits of L5-band signals while compensating its limitations.

A straightforward method to fulfill the target is integrating the L5-band measurements with the L1-band measurements through a proper weighting. Fig. 2 shows the weighting model for the conventional weighted-least-squares (WLS) positioning method (Realini & Reguzzoni, 2013), as well as the pseudorange errors of L1-band signals. In this paper, the pseudorange errors are estimated with the measurements and true locations of the receiver and a reference station by the double difference (DD) approach (Xu et al., 2019). The weighting surface based on C/N_0 and elevation approximates the pseudorange error in root-mean-square (RMSE), in order to adjust each measurement's weighting. As Fig. 2 shows, the model works well for L1-band measurement. However, the conventional weighting model developed for L1-band measurements may not fit the L5-band measurements, since they have different error behavior. Moreover, the enormous outliers, such as the NLOS receptions in urban, are also required to be detected and isolated before-hand. These challenges are the motivation of this research.

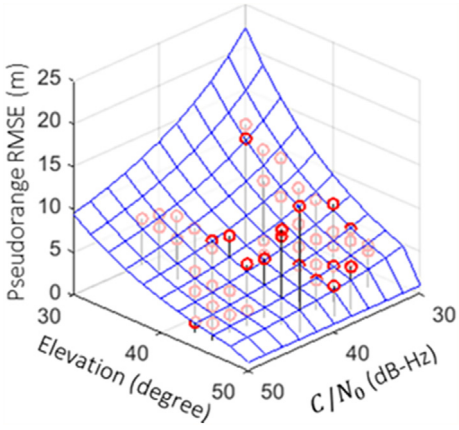

Fig. 2. The elevation angle and C/N_0 based weighting surface from goGPS (Realini & Reguzzoni, 2013), comparing to the pseudorange RMSE in an open-sky scenario. Pink and red circles denote the data is lower and higher than the surface, respectively. (For interpretation of the references to colour in this figure legend, the reader is referred to the web version of this article.)

3. Features for multipath and NLOS mitigation

3.1. Carrier-to-noise Ratio C/N_0

The C/N_0 in the GNSS measurement is an indicator of the received signal strength. Comparing to the direct signal, the power of the reflected signal will be reduced depending on the reflection coefficient (Suzuki & Kubo, 2012). As a result, the MP or NLOS degraded measurement may obtain a lower C/N_0, which can be identified by comparing with the C/N_0 behavior in the open-sky areas.

3.2. Elevation Angle El

The GNSS measurement performance is also related to the corresponding satellite elevation angle El. Shown with the skyplot in the urban area (Fig. 3), the satellite signal with a lower elevation has a high possibility of being blocked by the buildings, as the NLOS reception. On the

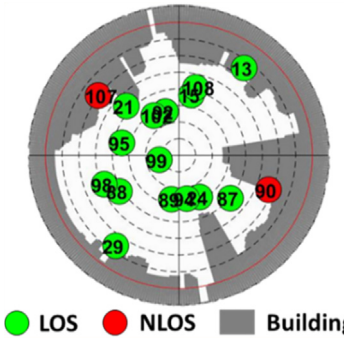

Fig. 3. The skyplot in an urban canyon. The green and red circles denote the LOS and NLOS signal, respectively. The shaded area denotes the surrounding buildings. (For interpretation of the references to colour in this figure legend, the reader is referred to the web version of this article.)

contrary, the satellite signal with a higher elevation is less likely to be blocked by buildings. Moreover, based on the law of reflection, the signal with higher elevation is harder to be reflected, since it requires the building being high enough to have a valid reflecting point (Hsu, 2018). Hence, the satellite elevation can be used as a feature indicating whether a measurement is reliable. In this study, an elevation mask of 10 degrees is employed to exclude the unreliable measurements beforehand.

3.3. dMP5

For the j^{th} satellite, the pseudorange and carrier phase measurements can be expressed as ρ_L^j and ϕ_L^j, respectively.

$$\rho_L^j = r^j + c\left(\delta t_u - \delta t^j\right) + I_L^j + T^j + \mathrm{E}_L^j \tag{1}$$

$$\phi_L^j = r^j + c\left(\delta t_u - \delta t^j\right) - I_L^j + T^j + \lambda_L N^{*j}_L + \varepsilon_L^j \tag{2}$$

where r is the actual range between receiver and satellite, δt_u is the receiver clock bias, δt^j is the satellite clock offset, I and the ionospheric error; T is the tropospheric error, λ is the wavelength. N^* is the phase ambiguity term, including the integer ambiguity, hardware biases and initial fractional terms. c is the speed of light. The signal type L equals to 1 for L1-band, or 5 for L5-band.E and ε denote other errors on the pseudorange and the carrier phase, respectively, including the measurement noise, multipath interference and NLOS delay. Since the ionospheric delay is related to the wavelength f_L of different signals (Leick et al., 2015), the L5-band ionospheric delay can be estimated by applying $\Phi_1^k - \Phi_5^k$, as follows.

$$I_5^j = \frac{\alpha}{\alpha - 1}\left(\phi_1^j - \lambda_1 N^{*j}_1 - \varepsilon_1^j - \phi_5^j + \lambda_5 N^{*j}_5 + \varepsilon_5^j\right) \tag{3}$$

where $\alpha = {f_1}^2/{f_5}^2$. Then, the variable $MP5$ is derived by applying $\rho_5^j - \Phi_5^j$ and substituting the preceding expression of I_5^j (Abou Galala et al., 2018; Estey & Meertens, 1999), as follows.

$$\begin{aligned} MP5 &\equiv \rho_5^j - \left(\tfrac{2\alpha}{\alpha-1}\right)\phi_1^j + \left(\tfrac{2\alpha}{\alpha-1} - 1\right)\phi_5^j \\ &= \mathrm{E}_5^j + \mathrm{B}_5^j - \left(\tfrac{2\alpha}{\alpha-1}\right)\varepsilon_1^j + \left(\tfrac{2\alpha}{\alpha-1} - 1\right)\varepsilon_5^j \end{aligned} \tag{4}$$

$$B_5^j = -\left(\frac{2\alpha}{\alpha-1}\right)\lambda_1 N^{*j}_1 + \left(\frac{2\alpha}{\alpha-1} - 1\right)\lambda_5 N^{*j}_5 \tag{5}$$

B_5^j is the ambiguity related term that remains a constant unless the occurrence of cycle slip. To eliminate the constant term, we derive a feature from the difference between the $MP5$ on adjacent epochs.

$$dMP5 = \Delta\mathrm{E}_5^j - \left(\frac{2\alpha}{\alpha-1}\right)\Delta\varepsilon_1^j + \left(\frac{2\alpha}{\alpha-1} - 1\right)\Delta\varepsilon_5^j \tag{6}$$

If the signal is not affected by reflections, the $dMP5$ feature will be small, which only contains the effect of measurement noise. For the signal with the MP or NLOS effect, the magnitude of the corresponding $dMP5$ will be significantly larger. Therefore, the $dMP5$ feature can be used to detect the MP or NLOS degraded measurements.

3.4. Pseudorange Residual

The conventional method for the GNSS positioning is to apply the iterative WLS with the pseudorange measurements, using

$$\Delta\mathbf{x} = \left(\mathbf{H}^{\mathrm{T}}\mathbf{W}\mathbf{H}\right)^{-1}\mathbf{H}^{\mathrm{T}}\mathbf{W}\Delta\rho \tag{7}$$

where the $\Delta\mathbf{x}$ is the state error, including the position difference and the receiver clock bias, $\mathbf{H}$ is the satellite geometry matrix, $\mathbf{W}$ is the weighting matrix, $\Delta\rho$ is the pseudorange measurement vector. Then, the pseudorange residual during estimation can be evaluated as follows (Hsu et al., 2017).

$$\widehat{\mathbf{E}}_{pr} = \Delta\rho - \mathbf{H}\cdot\Delta\mathbf{x} \tag{8}$$

where $\widehat{\mathbf{E}}_{pr} = \left(\widehat{\mathrm{E}}_L^1, \widehat{\mathrm{E}}_L^2, \cdots, \widehat{\mathrm{E}}_L^j\right)^T$ is the vector consist of the pseudorange residual for each satellite. The pseudorange residual indicates the consistency between the measurement and the estimation, which can be utilized to detect outliers.

4. The GNSS L1/L5 bands integrated positioning system with outlier exclusion

To improve the positioning performance in the urban area, a new GNSS L1/L5 bands integrated positioning algorithm is developed in this section. The flowchart is shown in Fig. 4. The main steps of the designed system include: 1) $dMP5$-based outlier exclusion; 2) L1/L5 bands integrated WLS positioning; 3) L1/L5 bands integrated consistency check.

4.1. dMP5-based Outlier Exclusion

Since the least-squares-based positioning method is sensitive to outliers, the feature $dMP5$ is employed to detect and exclude outliers in advance. The measurement with a $dMP5$ out of the interval $[\mu - 3\sigma, \mu + 3\sigma]$ will be identified as outliers. Here, based on the open-sky data, μ and σ are heuristically tuned as constant values of 6.3809×10^{-4} and 0.1034, respectively. After excluding the outlier, only the survived measurements are used for positioning.

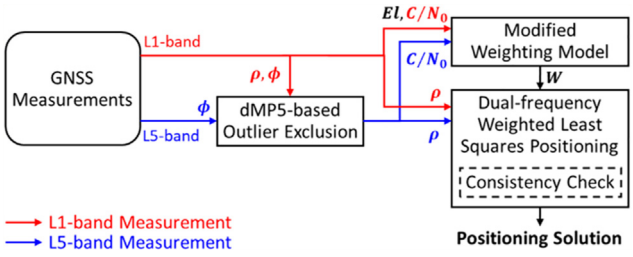

Fig. 4. The flowchart of the GNSS L1/L5 bands integrated positioning algorithm.

4.2. L1/L5 Bands Integrated WLS Positioning

The GNSS L5-band signal is naturally designed with a better positioning performance, comparing to the L1-band signal. In the developed system, only the L5-band measurement is used to estimate the user position if it is available for a satellite. However, the number of satellites supporting the L5-band signal is still limited in the current stage, resulting in a bad satellite geometry. To compensate for this limitation, we integrate the L5-band measurements with the measurements from L1-band only satellites during positioning. Here, the WLS positioning method is used to adjust the confidence of each measurement.

A modified weighting model is developed for the L1/L5 bands integrated measurements, thereby obtaining an appropriate weighting matrix during WLS positioning. Since the chip length of the L5-band signal is ten times shorter than the L1-band signal, the multipath effect on the L5-band measurement is also ten times smaller than the L1-band measurement. Hence, the RMSE of L5-band measurements can be approximated by the L1-band weighting model (Realini & Reguzzoni, 2013) with a tuning factor of 10, as follows.

$$\mathbf{W} = diag\left(\tau_L^1, \tau_L^2, \cdots, \tau_L^j\right)^{-1} \tag{9}$$

$$\tau_5 = \frac{1}{10}\left(\tau_1 - \tau_{1,open}\right) + \tau_{5,open} \tag{10}$$

$$\tau_1 = \begin{cases} \frac{1}{\sin^2 El}\left(10^{-\frac{CN_0 - T}{a}}\left(\left(\frac{A}{10^{\frac{F-T}{a}}} - 1\right)\frac{CN_0 - T}{F-T} + 1\right)\right), & CN_0 < T \\ 1, & CN_0 \geq T \end{cases} \tag{11}$$

where CN_0 denotes the satellite carrier-to-noise ratio C/N_0, τ_L^j is the measurement RMSE predicted from features C/N_0 and El.$\tau_{1,T} = \tau_{5,T} = 1$ denotes the τ_L^j of healthy measurements with $C/N_0 \geq T$. F defines the C/N_0 value of a measurement that is specifically weighted based on only the parameter A. a controls the bending of the surface. In this study, the parameters controlling the surface are tuned as $T = 50, F = 20, A = 50, a = 30$ based on experimental data, in order to make the model better fit the L1-band measurement behavior in the urban environment. Benefit from the reliability of the L5-band signal and the availability of the L1-band signal, the GNSS L1-band and L5-band measurements are complementarily integrated for a better positioning performance in urban areas.

4.3. L1/L5 Bands Integrated Consistency Check

During the WLS positioning, the GNSS measurements are normally within the user-equivalent range error (UERE) $\sigma_{UERE} \approx 7$ m (Kaplan & Hegarty, 2017), and consistent with each other to estimate the user positioning close to the actual location. However, a few measurements may be degraded by the MP or NLOS effect, introducing significant positioning error. These degraded measurements will be inconsistent with the estimation comparing to the healthy measurements, resulting in a large pseudorange residual $\widehat{\mathbf{E}}_L^j$. Then, the outliers can be detected based on the weighted sum of square residual Z, and comparing the $\sqrt{Z}$ with a chi-square test threshold Ψ by inverting the incomplete gamma function (Hsu et al., 2017; Walter & Enge, 1995) as follows.

$$Z = \widehat{\mathbf{E}}_{pr}{}^{\mathrm{T}}\mathbf{W}\widehat{\mathbf{E}}_{pr} \tag{12}$$

$$1 - P_{FA} = \frac{1}{\Gamma((J - N_{\Delta\mathbf{x}})/2)}\int_0^{\Psi^2} e^{-s} s^{\frac{J-N_{\Delta\mathbf{x}}}{2}} ds \tag{13}$$

where P_{FA} is the probability of false alarm given as 10^{-4}, J and $N_{\Delta\mathbf{x}}$ are the number of GNSS measurements and entries in the state vector, respectively. The measurement set with $\sqrt{Z} > \Psi$ will be identified as inconsistent and containing outliers. Then, the consistency can be improved by excluding the measurement that making the rest of measurements achieving the smallest $\sqrt{Z}$. The exclusion process will be repeated until the $\sqrt{Z}$ of the remaining measurements is lower than the threshold Ψ. Finally, the receiver positioning is estimated using those consistent enough measurements with the modified WLS method.

5. Positioning performance and analysis

5.1. Experiment setup

To demonstrate the performance of the designed methods, several experiments were conducted in different urban canyons of Hong Kong, as shown in Fig. 5 and Table 1. The measurements were collected with the RINEX format using the Allystar HD9300 GNSS receiver chip and their patched antenna Allystar AGR 6303. Noted that the ionospheric delay is different between L1-band and L5-band signals and hard to be modeled in the low latitude area. To better demonstrate the benefit from the L5-band signals, the user atmospheric delay is estimated and corrected based on the nearby reference station data. Assuming the GNSS measurements from the reference station are healthy, the receiver clock offset of the reference can be estimated by the least-squares positioning. By further

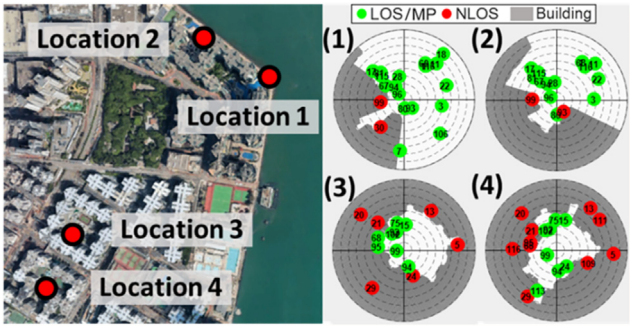

Fig. 5. Locations and sky-plots of different scenarios in the experiment.

Table 1
Characteristics of different Locations in the experiment.

Location	Scenario	Measurement Status
1	Away from one side buildings	Light multipath effects
2	Close to one side buildings	Severe multipath effects
3	Surrounded by buildings	Multipath/NLOS effects degraded
4	Surrounded by buildings	Severe Multipath/NLOS effects

knowing the reference station location, satellite position from the ephemeris, and the satellite clock offset from models (Kaplan & Hegarty, 2017), the atmospheric delay of each measurement on the reference station can be estimated from (1) as follows.

$$ATM_L^j = \rho_L^j - r^j + c\left(\delta t_u - \delta t^j\right) \tag{14}$$

The collected data were post-processed and compared the performance of different positioning algorithms on two-dimensional (East-West and South-North), including:

(1) L1-LS: Least squares positioning with L1-band measurements
(2) L5-LS: Least squares positioning with L5-band measurements
(3) L1/L5-LS: Least squares positioning with L1 and L5 bands measurements, the L1-band measurement is replaced by L5-band measurement if L5-band is available.
(4) L1-WLS: Conventional weighted least squares positioning ($T = 50, F = 10, A = 30, a = 30$) (Realini & Reguzzoni, 2013) with L1-band measurements
(5) DF-WLS: L1/L5-LS positioning method with the modified weighting scheme ($T = 50, F = 20, A = 50, a = 30$).
(6) DFE-CCWLS: the developed method combining DF-WLS with dMP5/consistency check based outlier exclusion.

5.2. Experiment results

The positioning performance of Location 1 is shown in Fig. 6 and Table 2. In this scenario, the average received satellite number is 19, including 9 satellites with L5-band measurements available. The multipath effect is small, resulting in a relatively accurate L1-band based positioning performance. Although the L5-band measurements are more accurate than L1-band, the L5-band measurement number is limited, which degrades the horizontal-DOP (HDOP) into 1.42. Therefore, the L5-LS only achieves an accuracy similar to L1-LS. By complementarily integrating the more accurate L5-band measurements with the L1-band measurements with healthy HDOP, the L1/L5-LS can achieve better performance. With a proper weighting between L1 and L5 bands, the DF-WLS enhance the accuracy into 1.8 m of RMSE. Finally, by employing the dMP5 feature to detect and exclude outliers, the DFE-CCWLS achieves the best accuracy, which is twice better than the conventional L1-band based methods. Although the HDOP of the DFE-CCWLS method is slightly increased due to the outlier exclusion, it is much smaller comparing to L5-LS and close to L1-LS, which guarantees a good positioning performance.

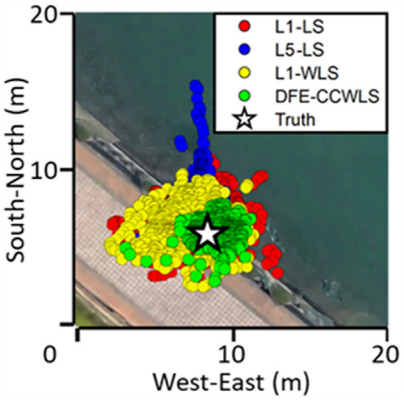

Fig. 6. The positioning results of Location 1, including the conventional L1-band only least-squares method (L1-LS), the L5-band only least squares method (L5-LS), the L1-band based weighted least squares method (L1-WLS) and the developed L1/L5 bands integrated weighted least squares method with outlier exclusion (DFE-CCWLS).

The positioning results of Location 2 are shown in Fig. 7 and Table 3. The average received satellite number is 17, including 8 satellites with L5-band measurements available. Since the receiver is close to tall buildings, the L1-band measurements are severely degraded by multipath effects and few NLOS receptions. Due to the limited measurement number and the large HDOP in the urban scenario, the L5-LS only achieves 10.2 m in RMSE. Without proper weighting, the performance of L1/L5-LS is even worse than the L1-WLS with C/N_0 and elevation based weighting. By employing the modified weighting between L1-band and L5-band measurements as well as the outlier exclusion scheme, the DFE-CCWLS enhances the accuracy into 6.3 m RMSE while maintaining 1.20 HDOP.

For Location 3 in dense urban, the positioning results are shown in Fig. 8 and Table 4. The average received satellite number is 14, while only 3 satellites in average support L5-band measurements. Since the buildings block many of the satellites, the L5-band measurement number is not sufficient for positioning. Moreover, using an equal weighting, the L1/L5-LS performance will be dominated by the accuracy of the L1-band measurements, which limits the benefits of L5-band. Due to the severe multipath effect in L1-band measurements, the L1-WLS fails to achieve accurate results by adjusting the weighting.

Differently, the DFE-CCWLS method complementarily integrates L1-band and L5-band measurements with proper weighting as well as excluding enormous outliers. Its positioning behaviors are shown in details as Fig. 9, including (a) the positioning error during different stages

Table 2
The 2D positioning RMSEs and HDOPs of different methods on location 1.

Method	L1-LS	L5-LS	L1/L5-LS	L1-WLS	DF-WLS	DFE-CCWLS
RMSE (m)	2.7	2.7	2.2	2.6	1.8	1.3
HDOP	0.76	1.42	0.76	0.76	0.76	0.84

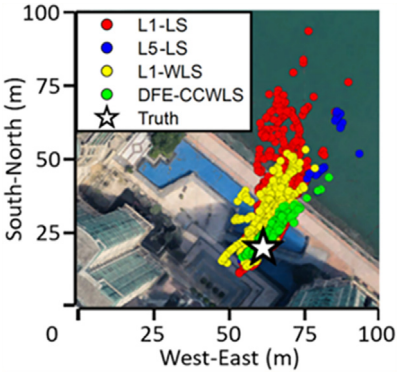

Fig. 7. Positioning results of different methods on Location 2.

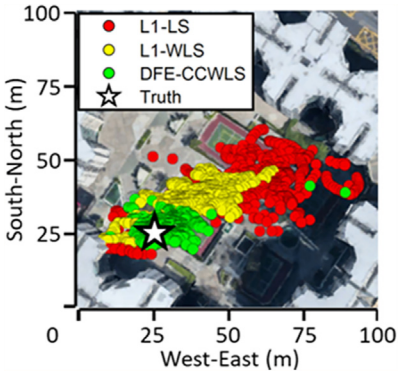

Fig. 8. Positioning results of different methods on Location 3.

of the DFE-CCWLS method; (b) the exclusion results using dMP5 feature or consistency check and the corresponding pseudorange errors; and (c) the measurement weighting assigned by the DFE-CCWLS method comparing to the pseudorange error. Here, DFE-WLS denotes the method only employs the dMP5-based outlier exclusion and the modified weighting scheme without consistency check. Through evaluating the dMP5 values, the L5-band measurements with higher error can be detected and excluded for slightly better positioning accuracy. By applying the consistency check, some enormous outliers can be further excluded. After that, the DFE-CCWLS method significantly deweights the measurements suffering huge errors, which achieves the best performance nearly three times better than that of the L1-WLS method. Note that the modified weighting is also employed during the consistency check. The measurements are consistent enough under the assigned weighting, even though some of the degraded measurements are not excluded. However, the DFE-CCWLS still contains enormous errors in few epochs. It is due to the miss-detection of NLOS measurements with an enormous error during consistency check when the available LOS measurements are very limited.

For Location 4, which is the most challenging environment, the positioning results are shown in Fig. 10 and Table 5. Here, the average received satellite number is 17, with 5 satellites supporting the L5-band measurements. The availability of L5-band measurements is limited, resulting in poor L5-LS performance. Besides, many of the L5-band measurements are severe NLOS receptions. The modified weighting scheme may mistakenly assign higher weights to those L5-band NLOS measurements than those L1-band LOS measurements. Hence, the DF-WLS method is unable to achieve better performance than L1-WLS. Since over half of the measurements are NLOS receptions, the consistency check may fail to detect outliers, or even worse, mistakenly exclude healthy measurements, which introduces enormous errors. As a result, the DFE-CCWLS method may not be able to improve the positioning performance in this harsh environment. In summary, the L5-band measurements have a great ability to resist the multipath effect, but still unable to solve the severe NLOS receptions.

5.3. Performance analysis

In this section, the performances of the L1-band and L5-band measurements from the same satellite are analyzed with different features. The pseudorange errors of L1-band and L5-band measurements on different locations (Fig. 5) are compared in Fig. 11. The measurements are classified into LOS/MP or NLOS based on the 3D building model and the ground-truth location. The accuracy of L1-band LOS/MP measurement is significantly degraded due to the multipath effects in the urban environment. However, the L5-band LOS/MP measurement from the same satellite achieves a much lower variance. Therefore, the

Table 3
The 2D positioning performances on location 2.

Method	L1-LS	L5-LS	L1/L5-LS	L1-WLS	DF-WLS	DFE-CCWLS
RMSE (m)	23.7	10.2	25.6	13.1	7.9	6.3
HDOP	1.06	4.38	1.06	1.06	1.06	1.20

Table 4
The 2D positioning performances on location 3.

Method	L1-LS	L5-LS	L1/L5-LS	L1-WLS	DF-WLS	DFE-CCWLS
RMSE (m)	39.7	n/a	40.2	20.5	9.6	7.5
HDOP	0.99	n/a	0.99	0.99	0.99	1.16

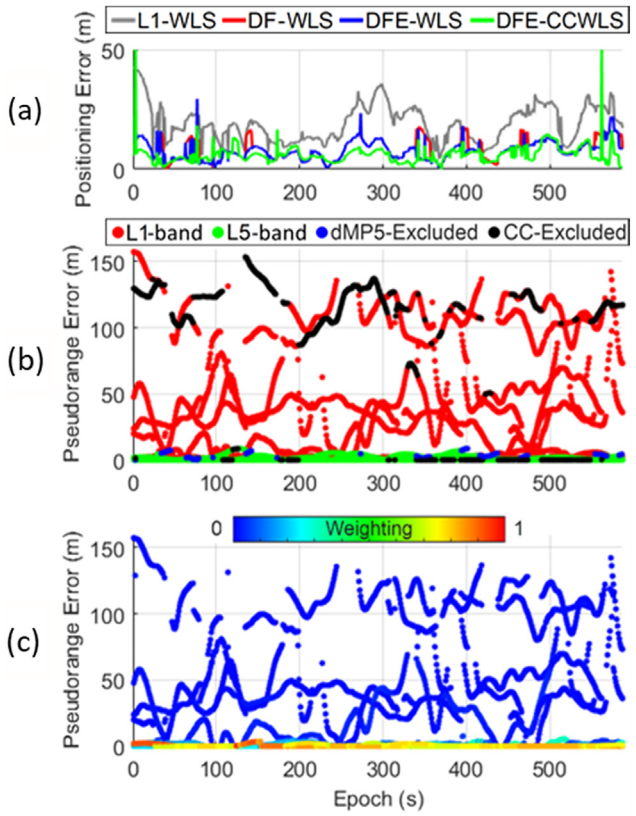

Fig. 9. The positioning behaviour details of the DFE-CCWLS method on Location 3, including (a) the positioning error during different stages; (b) the exclusion results using dMP5 feature or consistency check and the corresponding pseudorange errors; and (c) the measurement weighting assigned by the DFE-CCWLS method comparing to the pseudorange error.

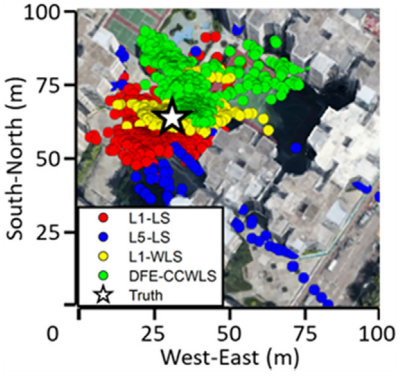

Fig. 10. Positioning results of different methods on Location 4.

L5-band measurements are naturally better in resisting multipath effects comparing to the L1-band measurements. For the NLOS measurements, although the L5-band signal has no contribution to reducing NLOS delay, the variance of the delay is significantly reduced. It is possibly due to the existence of multiple NLOS receptions in the urban areas. The final NLOS delay becomes a coupling effect of multiple reflected signals, namely the NLOS-multipath effect. Since the L5-band measurements are better on resisting multipath effects, the NLOS-multipath delay variance is significantly reduced, which is beneficial to outlier detection.

Then, the dMP5 features of the measurements on different locations are shown in Fig. 12. On all the locations, the dMP5 features of most healthy measurements are very close to zero and within the threshold. On the other hand, based on the dMP5 features exceeding the proposed threshold, many outliers can be correctly detected and excluded. The overall classification accuracy using dMP5 features is 96.8%, and 44.6% of the outliers can be correctly detected. Although 1.9% of the healthy measurements are mistakenly excluded as outliers, the measurement number is sufficient to maintain the positioning performance after combining L1-band measurements. A one-day experiment is also conducted in a dense urban environment to evaluate the performance of the dMP5 feature. The dMP5 values of different measurements during the experiment are shown in Fig. 13. The one-day experiment result is consistent with the preceding analysis, especially with Location 4, where most of the healthy measurements are within the dMP5 threshold. However, misclassification and miss-detection still occur when using the dMP5 feature to exclude outliers. Therefore, we further employ the consistency check in our method to exclude those remained NLOS measurements.

After that, the performance of the modified weighting model in the DFE-CCWLS is analyzed with respect to the pseudorange RMSE on the Location 1, 2 and 3 without severe NLOS receptions. Since the weighting scheme on both L1-band and L5-band measurements are modified comparing with the conventional L1-WLS method, the weighting performance on L1-band and L5-band measurements will both be analyzed. As Fig. 14 shows, the conventional model may under-estimate the L1-band pseudorange error from multipath effect or NLOS receptions in the urban environment. Moreover, the conventional model may over-estimate the RMSE of L5-band measurements, which is less affected by multipath interference. By providing different weighting based on the signal type, our modified weighting model can better approximate the

Table 5
The 2D positioning performances on location 4.

Method	L1-LS	L5-LS	L1/L5-LS	L1-WLS	DF-WLS	DFE-CCWLS
RMSE (m)	12.4	142.3	12.9	8.4	14.2	19.1
HDOP	0.76	6.96	0.76	0.76	0.76	0.91

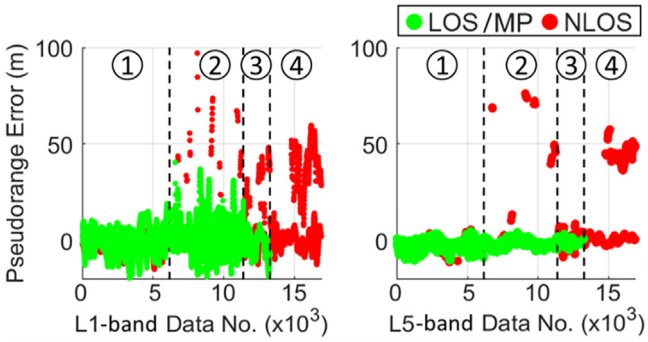

Fig. 11. The pseudorange errors of all the L1-band and L5-band measurements on different locations. The green markers denote the measurements from the visible satellites, including LOS and MP measurements. The red markers denote the measurements from the satellites blocked by buildings, possibly NLOS receptions. (For interpretation of the references to colour in this figure legend, the reader is referred to the web version of this article.)

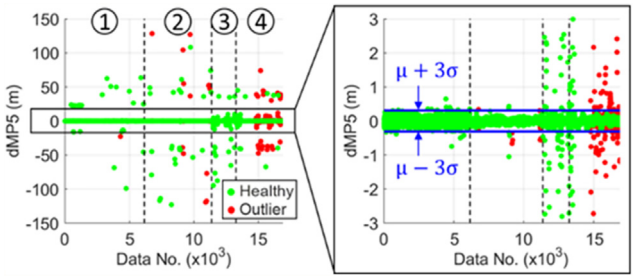

Fig. 12. The dMP5 value of measurements on different locations. The measurements with pseudorange errors below 10 m are denoted as healthy measurements with green markers. Otherwise, the measurements are denoted as outliers with red markers. The blue lines on the right denote the threshold used to detect outliers. (For interpretation of the references to colour in this figure legend, the reader is referred to the web version of this article.)

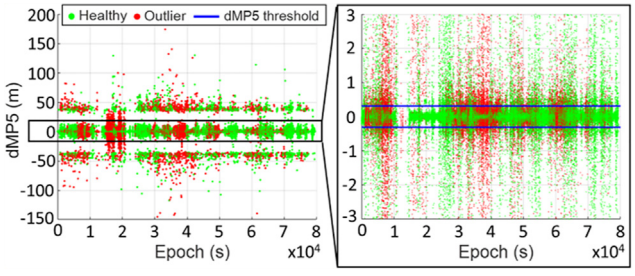

Fig. 13. The dMP5 values of all the measurements during the one-day experiment.

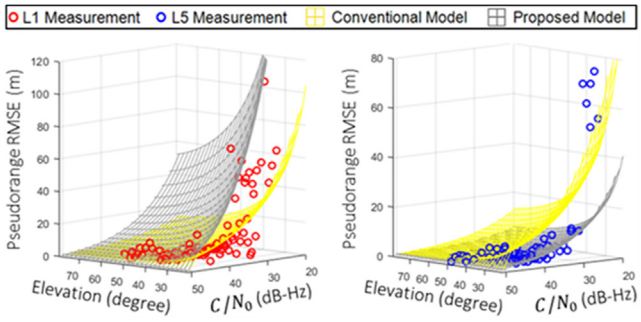

Fig. 14. The C/N_0 and El based weighting surface of the conventional model and the modified model with respect to the pseudorange RMSE.

pseudorange RMSE in urban for both L1-band and L5-band measurements. Noted that some of the L5-band measurements are severe NLOS receptions and unable to be appropriately deweighted. However, these outliers are very inconsistent with most of the L5-band measurements. Therefore, the outliers can be easily detected and excluded by the consistency check.

Finally, the pseudorange residuals during the modified WLS positioning are analyzed to evaluate its performance on outlier detection. As Fig. 15 shows, due to the multipath effects, the L1-band measurements are inconsistent, resulting in large residuals. On some epochs, the residuals of the LOS/MP measurements can be even larger than that of the NLOS measurements. Hence, it is difficult to detect NLOS receptions based on pseudorange residuals. Since the L5-band measurements are better on resisting multipath effects, most of the measurements are healthy and consistent, except NLOS receptions. Therefore, the NLOS receptions can be easily detected by abnormally large residuals. However, for Location 4, where most of the L5-band measurements are NLOS receptions, the pseudorange residuals

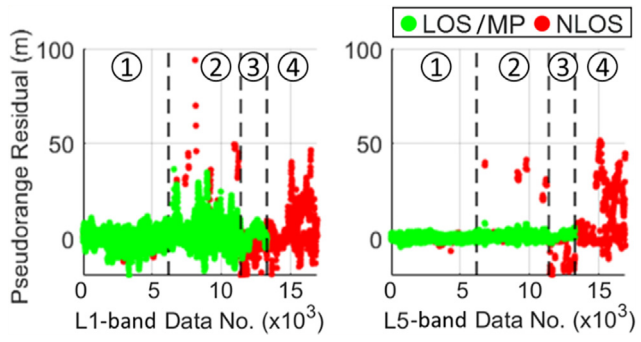

Fig. 15. The pseudorange residual of each measurement during the modified WLS positioning on different locations.

of all the measurements have similar magnitudes and overlapped. Although some of the measurements may have fewer errors, it is hard to be distinguished by the residuals. In summary, with better multipath effect resistance, the L5-band measurements can improve the performance of outlier exclusion. However, its performance is still similar to L1-band measurements for the location with severe NLOS receptions.

5.4. Dynamic experiment result

A dynamic experiment is conducted to validate the developed DFE-CCWLS method for more general cases. The GNSS receiver is mounted on top of the vehicle, which is driven in a dense urban environment. The true location of the vehicle is recorded by the solution from the high-end GNSS/INS integrated navigation sensor (NovAtel SPAN-CPT). The experiment trajectory and the solutions from different methods are shown in Fig. 16. The 2D positioning error and received satellite numbers during the experiment are shown in Fig. 17. The overall positioning performance is summarized in Table 6. By assigning different weights on measurements, the L1-WLS can improve the positioning accuracy from 37.2 m to 31.1 m of RMSE. In this dense urban scenario, the DF-WLS may mistakenly increase the weighting of some NLOS degraded L5-band measurement, resulting in a positioning performance worse than the L1-WLS method. However, by employing the dMP5 feature and consistency check to exclude NLOS measurements, the DFE-CCWLS method can make use of the modified weighting scheme and achieve the best overall performance. Especially around epoch 111, three measurements are containing nearly 100 m NLOS errors. Two of them are L5-band measurements excluded by the dMP5 feature and consistency check, respectively. The remaining one is the L1-band measurement, which will be significantly deweighted by the modified weighting scheme. Hence, the DFE-CCWLS performs much better than the L1-WLS around that period. Nevertheless, the DFE-CCWLS sometimes still introduces enormous errors due to the miss-detection of the NLOS measurements when nearly half of the measurements are NLOS receptions.

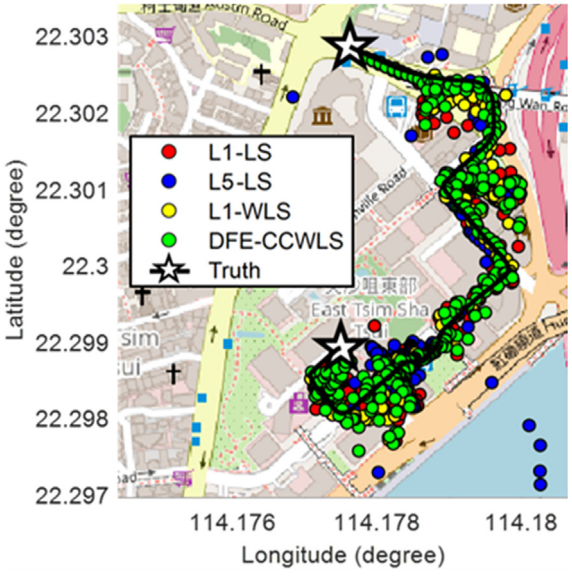

Fig. 16. Positioning results of different methods in the dynamic test.

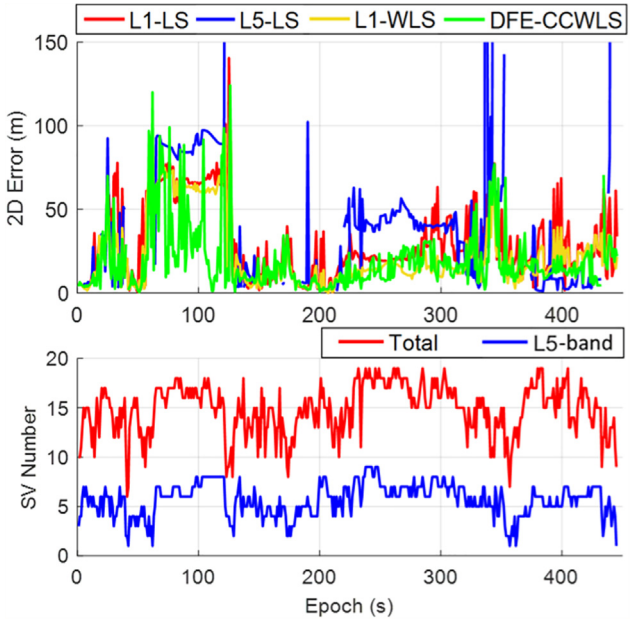

Fig. 17. Comparison of the 2D positioning errors from different methods during the dynamic experiment.

6. Conclusions and future work

In this study, a new GNSS L1/L5 bands integrated positioning algorithm with outlier isolation is developed for receivers used in urban areas. The developed DFE-CCWLS method firstly employs the dMP5 feature to exclude 44.6% of the outliers before positioning. After that, a modified weighting scheme is employed to assign different weights on L1-band or L5-band measurements based on the C/N_0 and El. The modified weighting scheme can appropriately down-weight the measurements with enormous pseudorange errors in order to improve the positioning performance. Finally, we apply the consistency check during the modified WLS positioning to detect and isolate the outliers, possibly NLOS receptions. As a result, the DFE-CCWLS method can significantly improve the positioning accuracy for the urban scenarios. For the urban scenarios without severe NLOS receptions, the DFE-CCWLS method achieves a positioning RMSE less than 10 m, which is at least twice better than that of the conventional method.

Due to the limited availability of the L5-band supported satellites in the urban area, it is hard to compare the L5-band measurement performance from different constellations. The comparison between constellations will be con-

Table 6
The 2D positioning performances during the dynamic experiment.

Method	L1-LS	L5-LS	L1/L5-LS	L1-WLS	DF-WLS	DFE-CCWLS
RMSE (m)	37.2	128.6	37.5	31.1	33.5	27.1
HDOP	0.99	3.83	0.99	0.99	0.99	1.21

ducted in the future when more satellites are supporting the L5-band signal. Although the L5-band measurement has great benefits on resisting multipath effect, it is still unable to solve severe NLOS receptions. Different from the DFE-CCWLS method, the 3DMA GNSS positioning method has an excellent performance in terms of NLOS mitigation but less effective with multipath effects. The 3DMA GNSS ray-tracing technique can correct the NLOS delay based on the surrounding building geometries, achieving the positioning performance with less than 10 m error in the urban scenario. However, the multipath effect is related to the phase change of the reflected signal, which is hard to be appropriately modeled by 3DMA GNSS. Therefore, the complementary integration of the DFE-CCWLS and the 3DMA GNSS is worth to be studied in the future.

Declaration of Competing Interest

The authors declare that they have no known competing financial interests or personal relationships that could have appeared to influence the work reported in this paper.

Acknowledgements

This work was supported in part by the Hong Kong Polytechnic University startup fund under the project 1-ZVKZ, "Positioning and Navigation for Autonomous Driving Vehicle by Sensor Integration".

References

Abou Galala, M., Kaloop, M.R., Rabah, M.M., et al., 2018. Improving precise point positioning convergence time through TEQC multipath linear combination. J. Surv. Eng. 144 (2), 04018002.

Basiri, A., Lohan, E.S., Pedro Figueiredo e, S., et al., 2014. Overview of positioning technologies from fitness-to-purpose point of view. In: International Conference on Localization and GNSS 2014 (ICL-GNSS 2014), 2014, pp. 1–7.

Chen, L., Thombre, S., Järvinen, K., et al., 2017. Robustness, security and privacy in location-based services for future IoT: a survey. IEEE Access 5, 8956–8977. https://doi.org/10.1109/ACCESS.2017.2695525.

Chen, X., 2018. Statistical multipath model comparative analysis of different GNSS orbits in static urban canyon environment. Adv. Space Res. 62 (5), 1034–1048. https://doi.org/10.1016/j.asr.2018.06.005.

Crosta, P., Zoccarato, P., Lucas, R., et al., 2018. Dual frequency mass-market chips: test results and ways to optimize PVT performance. In: Proceedings of the 31st International Technical Meeting of the Satellite Division of The Institute of Navigation (ION GNSS+ 2018), 2018, pp. 323–333.

Deo, M., El-Mowafy, A., 2018. Triple-frequency GNSS models for PPP with float ambiguity estimation: performance comparison using GPS. Survey Rev. 50 (360), 249–261. https://doi.org/10.1080/00396265.2016.1263179.

El-Mowafy, A., 2017. Advanced receiver autonomous integrity monitoring using triple frequency data with a focus on treatment of biases. Adv. Space Res. 59 (8), 2148–2157. https://doi.org/10.1016/j.asr.2017.01.037.

Estey, L.H., Meertens, C.M., 1999. TEQC: the multi-purpose toolkit for GPS/GLONASS data. GPS Solutions 3 (1), 42–49.

Ge, Y., Yang, X., Qin, W., et al., 2019. Mitigation of the multipath effect in BDS-based time transfer using a wave-absorbing shield. Adv. Space Res. 63 (9), 2771–2783. https://doi.org/10.1016/j.asr.2018.05.008.

Groves, P., 2013. Multipath vs. NLOS signals. Inside GNSS 8 (6), 40–42.

Groves, P., Jiang, Z., 2013. Height aiding, C/N 0 weighting and consistency checking for GNSS NLOS and multipath mitigation in urban areas. J. Navigation 66 (5), 653–669.

Groves, P., Jiang, Z., Skelton, B., et al. (2010). Novel multipath mitigation methods using a dual-polarization antenna. In: Proceedings of the 23rd International Technical Meeting of the Satellite Division of The Institute of Navigation (ION GNSS 2010), 2010, pp. 140–151.

Guo, F., Zhang, X., Wang, J., et al., 2016. Modeling and assessment of triple-frequency BDS precise point positioning. J. Geod. 90 (11), 1223–1235. https://doi.org/10.1007/s00190-016-0920-y.

Hsu, L.-T., 2018. Analysis and modeling GPS NLOS effect in highly urbanized area. GPS Solutions 22 (1), 7.

Hsu, L.-T., Gu, Y., Kamijo, S., 2015a. NLOS correction/exclusion for GNSS measurement using RAIM and city building models. Sensors 15 (7), 17329–17349.

Hsu, L.-T., Gu, Y., Kamijo, S., 2016. 3D building model-based pedestrian positioning method using GPS/GLONASS/QZSS and its reliability calculation. GPS Solutions 20 (3), 413–428. https://doi.org/10.1007/s10291-015-0451-7.

Hsu, L.-T., Tokura, H., Kubo, N., et al., 2017. Multiple faulty GNSS measurement exclusion based on consistency check in urban canyons. IEEE Sens. J. 17 (6), 1909–1917.

Hsu, L.-T., Yanlei, G., Shunsuke, K., 2015b. Pedestrian localization service using 3D map and RAIM GNSS satellite selection technique. In: 2015 IEEE 18th International Conference on Intelligent Transportation Systems, 2015b, pp. 1377–1382.

Jiang, Z., Groves, P.D., 2014. NLOS GPS signal detection using a dual-polarisation antenna. GPS Solutions 18 (1), 15–26.

Kaplan, E., Hegarty, C., 2017. Undestanding GPS/GNSS: Principles and Applications, 3rd ed. Artech House.

Küpper, A., 2005. Location-Based Services: Fundamentals and Operation. John Wiley & Sons.

Leclère, J., Landry, R., Botteron, C., 2018. Comparison of L1 and L5 bands GNSS signals acquisition. Sensors 18 (9), 2779.

Leick, A., Rapoport, L., Tatarnikov, D., 2015. GPS satellite surveying. John Wiley & Sons.

Li, B., Shen, Y., Zhang, X., 2013. Three frequency GNSS navigation prospect demonstrated with semi-simulated data. Adv. Space Res. 51 (7), 1175–1185. https://doi.org/10.1016/j.asr.2012.10.031.

Lohan, E.S., Borre, K., 2016. Accuracy limits in multi-GNSS. IEEE Trans. Aerosp. Electron. Syst. 52 (5), 2477–2494. https://doi.org/10.1109/TAES.2016.150241.

Luo, X., Li, S., Xu, H., 2016. Results of real-time kinematic positioning based on real GPS L5 data. IEEE Geosci. Remote Sens. Lett. 13 (8), 1193–1197. https://doi.org/10.1109/LGRS.2016.2575062.

Meurer, M., Erker, S., Tholert, S., et al., 2009. GPS L5 first light: a preliminary analysis of SVN49's demonstration signal. (INNOVATION). GPS World 20 (6), 49.

Ng, H.F., Zhang, G., Hsu, L.-T., 2019. A computation effective range-based 3D mapping aided GNSS with NLOS correction method. J. Navig.

Nobuaki, K., Kaito, K., Li-Ta, H., et al., 2017. Multipath mitigation technique under strong multipath environment using multiple antennas. J. Aeronaut., Astronaut. Aviation 49 (1), 75–82. https://doi.org/10.6125/17-0130-928.

Qin, H., Liu, P., Cong, L., et al., 2019. Triple-frequency combining observation models and performance in precise point positioning using real BDS data. IEEE Access 7, 69826–69836. https://doi.org/10.1109/ACCESS.2019.2918987.

Realini, E., Reguzzoni, M., 2013. goGPS: open source software for enhancing the accuracy of low-cost receivers by single-frequency relative kinematic positioning. Meas. Sci. Technol. 24 (11) 115010.

Seco-Granados, G., Fernandez-Rubio, J.A., Fernandez-Prades, C., 2005. ML estimator and hybrid beamformer for multipath and interference mitigation in GNSS receivers. IEEE Trans. Signal Process. 53 (3), 1194–1208. https://doi.org/10.1109/TSP.2004.842193.

Spilker Jr, J.J., Van Dierendonck, A.J., 2001. Proposed New L5 Civil GPS Codes. Navigation 48 (3), 135–143. https://doi.org/10.1002/j.2161-4296.2001.tb00237.x.

Strode, P.R.R., Groves, P.D., 2016. GNSS multipath detection using three-frequency signal-to-noise measurements. GPS Solutions 20 (3), 399–412. https://doi.org/10.1007/s10291-015-0449-1.

Suzuki, T., Kubo, N., 2012. GNSS positioning with multipath simulation using 3D surface model in urban canyon. In: Proceedings of the 25th International Technical Meeting of The Satellite Division of the Institute of Navigation (ION GNSS 2012), 2012, pp. 438–447.

Tabibi, S., Nievinski, F.G., van Dam, T., et al., 2015. Assessment of modernized GPS L5 SNR for ground-based multipath reflectometry applications. Adv. Space Res. 55 (4), 1104–1116. https://doi.org/10.1016/j.asr.2014.11.019.

Türk, T., 2006. Location Based Services (LBS) and Related Standards. International Symposium on Geospatial Databases for Sustainable Development, 2006.

van der Marel, H., de Bakker, P.F., 2012. Single- versus dual-frequency precise point positioning. InsideGNSS, 30–35.

Walter, T., Enge, P., 1995. Weighted RAIM for precision approach. In: Proceedings of the 8th International Technical Meeting of the Satellite Division of The Institute of Navigation (ION GPS 1995), 1995, pp. 1995–2004.

Wang, L., Groves, P.D., Ziebart, M.K., 2015. Smartphone shadow matching for better cross-street GNSS positioning in urban environments. J. Navig. 68 (3), 411–433. https://doi.org/10.1017/S0373463314000836.

Warnant, R., Vyvere, L.V.D., Warnant, Q., 2018. Positioning with single and dual frequency smartphones running Android 7 or later. In: Proceedings of the 31st International Technical Meeting of the Satellite Division of The Institute of Navigation (ION GNSS+ 2018), 2018, pp. 284–303.

Xu, B., Jia, Q., Luo, Y., et al., 2019. Intelligent GPS L1 LOS/Multipath/NLOS Classifiers Based on Correlator-, RINEX-and NMEA-Level Measurements. Remote Sens. 11 (16), 1851.

Zhang, Q., Chen, Z., Rong, F., et al., 2019. Preliminary availability assessment of multi-GNSS: a global scale analysis. IEEE Access 7, 146813–146820. https://doi.org/10.1109/ACCESS.2019.2946221.

Zhu, N., Marais, J., Bétaille, D., et al., 2018. GNSS position integrity in urban environments: a review of literature. IEEE Trans. Intell. Transp. Syst. 19 (9), 2762–2778. https://doi.org/10.1109/TITS.2017.2766768.

Zumberge, J., Heflin, M., Jefferson, D., et al., 1997. Precise point positioning for the efficient and robust analysis of GPS data from large networks. J. Geophys. Res. Solid Earth 102 (B3), 5005–5017.